Welding in the World
https://doi.org/10.1007/s40194-025-02307-9

RESEARCH PAPER

Generalization of convolutional neural networks for defect detection in friction stir welding towards the qualification of a spindle-integrated high granularity process-force measurement system

P. Rabe[1] · A. Schiebahn[1] · U. Reisgen[1] · A. Strachkov[2] · M. Fey[2] · C. Brecher[2]

Received: 19 September 2025 / Accepted: 19 December 2025

Abstract
Friction Stir Welding (FSW) is a solid-state welding process, which has strongly impacted welding technology, particularly for aluminum alloy applications. Reliable in-line process monitoring is not yet available for most common defects and downstream non-destructive and intermittent destructive testing are generally employed to validate weld seam quality. To reduce cost and production time significant efforts have been undertaken in the recent past to develop process-monitoring systems for FSW based on the evaluation of transient process-data. Neural Networks have been used widely to analyse FSW-process data and evaluate the process characteristics or weld seam quality. The data analysed includes welding parameters, thermal-/acoustic-measurement, image or video data and, most notably, the distinct and descriptive process feedback forces and torque. In this study, conducted within the scope of RWTH Aachen's Cluster of Excellence (Internet of Production), a high granularity direct force measurement setup, which was adapted to the production environment, by integrating reliable, cost-efficient sensors into the machining spindle, was used. Weld data was recorded over a wide range of FSW applications with varying weld-parameters and Al-alloys. Convolutional Neural Networks (CNN) that were previously developed based on measurements of external force and torque sensors were adapted to evaluate the higher granularity data of the new sensor-system and detect volumetric defects within the welds. Good generalization was shown across the weld parameter sets, alloys and welding tool. An average classification accuracy of 98.04% was achieved over three network trainings. Due to the segmentation of data for the evaluation 100% of internal defects were successfully detected by each network iteration. The developed solution aims at offering a highly reliable, spindle integrated and cost-efficient quality monitoring solution for FSW to replace the required expensive and time-consuming testing.

Keywords Friction stir welding · Quality monitoring · Deep neural network

1 Introduction

The research presented within this publication is part of the interdisciplinary, collaborative Cluster of Excellence Framework "Internet of Production" of RWTH Aachen University. The superior goal is the digitalization of complete production chains [1]. This publication is a continuation of previously published research in developing a generalized defect detection solution with a wide application range and low barrier of application. The experimental methodology has previously been established, allowing for comparison of the achieved results. The major new developments in this paper relate to the data-acquisition system, its granularity and the influence of measured variables and relation to the accuracy

Recommended for publication by Commission III - Resistance Welding, Solid State Welding, and Allied Joining Process.

✉ P. Rabe
pascal.rabe@isf.rwth-aachen.de

[1] Welding and Joining Institute, RWTH Aachen University, Pontstraße 49, 52062 Aachen, Germany

[2] Laboratory for Machine Tools and Production Engineering: Werkzeugmaschinenlabor der RWTH Aachen University, Steinbachstr. 19, 52074 Aachen, Germany

Published online: 19 January 2026

of quality determination. The fundamental motivation of the project and used methodology are constant along development path and accompanying publications, which therefore overlap in the in the chapters regarding introduction, motivation, state of the art and experimental setup [2–6]. A detailed list of new research aspects and inherited methodology aspects is given at the end of this chapter.

Friction Stir Welding (FSW) was developed by The Welding Institute (TWI) and patented in 1991 [7]. This advanced solid-state welding process enables high quality welding through intermixing of materials in a plastic state and subsequent dynamic recrystallization, driven by frictional heat and pressure generated by a rotating, non-consumable welding tool. Joining in the solid phase mitigates the challenges conventionally associated with fusion welding processes for aluminum alloys, resulting in a refined microstructure. The reduced specific energy input contributes to enhanced mechanical and technological properties, alongside the energy efficiency, making FSW a favored joining process in the aerospace and rolling stock industries [8]. The growth of electromobility in conjunction with efforts in light weight construction across all transportation sectors has increased the number of FSW applications. Many developments and applications are centered around battery trays, heat exchangers and mixed material joints of copper and aluminum for electrical power systems [9, 10]. For FSW industrial quality control is realized thorough downstream testing methods, introducing extra process steps and an increase in production time and cost. The increasing number and diversification of applications, coupled with a rise in production volume necessitates the development of reliable and cost-efficient non-destructive inline quality monitoring for FSW [11].

In current industrial production specialized FSW welding machines, capable of automated welding with closed loop axial force control to adaptively control the welding process are most commonly used. The machines are equipped with sensors to monitor the axial force and other welding parameters to enable the closed, adaptive control loop.

Variations in sensor selection, accuracy, recording frequency and latency between different manufacturers and machines result in insufficient process force feedback for efficient monitoring of the FSW's dynamic process behavior. The limitations associated with direct measurements and internal sensor systems have led to the use of external sensors to research and develop correlations between the dynamic characteristics of the FSW process, recorded transient data and weld-seam quality [2, 12–15]. The majority of published research utilizes analysis of the dynamic force components of the in-plane welding force feedback or variations of the axial force or torque. A defect detection is generally achieved despite varying methods of analysis and recorded variables. However, most defect detection systems are limited in their applicability to a single joining task with fixed alloy, sheet thickness, welding tool and often a single weld parameter combination.

In previous works the detection of internal volumetric defects based on transient process data was developed, a system based on Convolutional Neural Networks (CNN) was used, its generalization between welding tasks was addressed and the possibility of transfer between different types of welding machines was shown [2, 3]. To further increase applicability this publication focuses on the used measuring system. The previously employed external system, which was expensive and offered limited data granularity, is replaced by a spindle-integrated solution. The SpindleForce measurement system enables real-time measurement of process forces. It was initially designed for the characterization of milling processes across a wide frequency range. The new system provides direct force measurement based on cost-efficient and reliable sensors integrated directly into the main spindle, offering an industry-ready solution that remains robust in typical production environments [16].

Today the FSW process is regarded as comparably stable and well controllable in industrial production environments. Despite this FSW is susceptible to numerous external disturbances and variations of workpieces and operational conditions, which can induce defects in the resulting weld seam. Some of the defects may remain undetected by the most commonly used quality monitoring techniques, such as axial force monitoring and visual inspection. [17]

The factors influencing process stability can be separated into welding parameter-based factors, welding machine properties and workpiece irregularities. When monitoring FSW weld quality the machine properties can be regarded as constant and only need to be parameterized when developing generalized solutions [18]. The welding tool presents a special case, as it is a constant factor in most development cycles, but needs to be included for production environments, as tool wear significantly influences resulting process forces, their dynamic behavior and the resulting weld seam quality [19, 20]. In FSW the primary welding parameters, spindle speed, feed rate and axial force, are generally established though empirical methods and remain fixed for each specific welding task. As these are resilient against outside influence, significant disturbances are not primarily attributed to these parameters, but rather to their interaction with the workpiece, which can induce process deviations that result in defects. The most prevalent irregularities in workpieces are gap tolerances, thickness variations, hardness gradients, and surface condition changes [21]. Changes in hardness, thickness variations and gap tolerances influence the material volume underneath the welding tool, changing the heat input condition, material plastization, resulting transport of material by the tool and weld seam formation. This negative interplay can result in process instabilities and weld seam defects [21].Surface conditions of tool and

workpiece have significant impact on the interface condition, heat input and material transport through wear state, adhesion and friction coefficient [22]. Each of these factors or their combinations can contribute to deviations from a steady cyclical state. The deviations can induce a process state during which conventional quality control measures fail to detect defects occurring during weld seam formation.

Two primary mechanisms for defect initiation have been identified based on the relation of influences on weld quality. Plunge depth significantly affects heat generation and material transport. It can reliably be monitored through internal machine data and related to weld quality. Variations in plunge depth are a result of multiple factors, leading to either an increase or decrease in resulting depth, which can result in incomplete penetration and compromised weld properties [23]. Increased plunge depth leads to close proximity or direct contact between tool and backing, potentially causing adhesion, backing plate or tool failure or defects induced by excessive temperatures and abnormal material transport.

The second identified mechanism is considerably more challenging to detect using current quality monitoring solutions. Defects are caused by irregular material flow within the stir zone. The periodically oscillating process condition and resulting intermittent material transport around the welding tool are mainly driven by the specific energy input and tool geometry and can be influenced by changes of multiple process variables. Energy input is influenced by process parameters as well as the interface condition, workpiece strength/thickness, or tool wear. Significant changes in specific energy input, higher as well as lower, can disrupt the weld seam formation by reducing material flow around the tool [24, 25]. Insufficient material transport may lead to local or prolonged internal volumetric defects within friction stir welded (FSW) seams, such as voids, cavities, or surface imperfections. Due to these defect occurrences, FSW production using current process control and quality monitoring generally requires downstream quality inspection. These additional quality control measures add complexity, time and cost to the FSW-production chain.

Due to the added cost and time significant efforts have been made by many researchers to develop quality monitoring systems based on process data. The friction-based heat input at the tool workpiece interface and translational movement of the tool through the plasticized material result in comparatively high process forces, which are commonly used to characterize the process. During welding the process forces consist of static and dynamic components in all three spatial directions. In a steady welding state the forces oscillate cyclically, corresponding to the rotational speed of the welding tool and its higher harmonics [26]. While the cyclical oscillation of spatial forces at the spindle-imprinted frequency is commonly known, numerous influencing factors, interdependencies, and relationships to force amplitude, occurrence of higher harmonics, material transport, as well as dependencies on welding parameters, tools, and workpiece properties remain inadequately understood or quantified. Many studies have focused on establishing correlations between the measured oscillation, their temporal deviations and weld seam quality, despite the uncertain causes of the phenomena. Many different solutions have been proposed to relate weld quality to deviations of forces and torque oscillations, e.g. [3, 6, 12, 13, 27–30]. These proposed solutions are based on the proven hypothesis that the majority of process parameters and disturbances are condensed in the recordable process force feedback. Therefore, a representation of the process's dynamic behavior and induced deviations and instabilities can be drawn. Based on this compounded representation of the process state an indication towards weld quality can then be derived.

Numerous authors demonstrate the potential for empirical anomaly detection through process force feedback evaluation. The analysis primarily relies on extracted incremental features or gradual changes within the recorded data. Most studies focus on variations of the dynamic oscillations or combinations of changes in static and dynamic force components. Jene's correlation of weld defects is however based on the mean average lateral force [30]. Further research into the empirical evaluation of process forces [12, 28] confirms the feasibility of assessing dynamic components while highlighting limitations and the necessity to adjust evaluations and selected features for each change in welding conditions, which restricts industrial applicability. Besides the time domain analytical correlations can be identified in the frequency domain. Gebhard analyzed frequency spectra and determined that high levels of low frequency oscillation can indicate internal void defects [18].

For the first application of Artificial Neural Networks (ANN) to detect internal welding defects in FSW Boldsaikhan et al. also utilized frequency domain data [31]. A Fully Connected Neural Network (FCNN) was trained with the frequency domain data of welding torque recorded at 51.2 Hz. The FCNN could identify internal weld defects in a dataset heavily biased towards defect free (96.6%) welds. Subsequent work demonstrates the application of wavelet transformations of the in-plane forces to evaluate weld quality using ANNs [29]. 95% of internal defects greater than 0.08 mm of the test dataset were identified correctly by a FCNN. Further advancements in AI-technology, particularly deep learning techniques, enabled Hartl et al. [32] to classify FSW-welds using surface images and weld force data by using Convolutional Neural Networks (CNN). Classification accuracies up to 79,2% were achieved by CNN based on the Alex-Net [33] architecture.

Multiple different solutions have demonstrated success in correlating dynamic process behavior with FSW weld quality. The studies shown are all limited in applicability

as they do not provide generalized solutions across different alloys, workpiece thicknesses and multiple welding tools. Overall, the possibility of detection of internal weld defects through force feedback analysis has been validated. Despite this progress, most current methods remain inapplicable to industrial production requirements. Preparation of the necessary datasets for training of Neural Networks (NN) involves significant effort, as extensive test welds with sufficient variation must be produced, prepared and labeled for each welding task.

The systems used to record weld data, forces, torque, currents, vibrations, etc., at high granularity must be added to the welding fixture or tool holder. Restricting the possibility of implementation into FSW-production. These high frequency, high fidelity devices are generally expensive to acquire and implement, often also requiring special expertise in operation, recording and data evaluation, making them cost prohibitive for industrial production environments.

For this study the methodology of previous studies was retained. While the previous developments focused increases in classification accuracy and generalization between welding tasks [3, 4], as well applicability through welding machine transfer [2] the current publication aims to improve data acquisition at high granularity and lowered cost and implementation requirements. To achieve this goal a robust and wear-free spindle integrated measurement system based on eddy current sensors with high measurement granularity of all spatial force was used. The system does not limit accessibility and provides a comparatively cheap measurement solution based on industrially established principles and devices.

The major new aspects evaluated within this paper are listed in Table 1 and generally regard the evaluated, industrially applicable measurement system, as well as further evaluation of the NN classification data and results.

2 Experimental setup and data-acquisition

The welding experiments were performed on a 5-Axis machining center, Heller HF3500. The machine is equipped with a WEISS Spindle with 40 kW and a maximum spindle speed of 18,000 RPM. The workpieces were rigidly clamped to a 10 mm mild steel backing plate. The mill scale of the backing plate was retained to efficiently prevent adhesion of the workpiece, resulting in increased roughness of the weld root surface. Workpiece dimensions were $500 \times 150 \text{x} 1.5\ \text{mm}^3$ allowing for multiple parallel welds of 440 mm length on the same plate. To prevent the influence of edge shape and gaps between plates, the welds were performed as full penetration seam on plate welds. Workpieces of three different aluminum alloys were used for the experiments. Alloys AW5754-H22, AW6005-T4, AW7075-T6 were chosen to include a wide range of FSW applications and industries using FSW. The welding tools were fabricated from H13 tool steel and heat treated to achieve a hardness of 600 ± 10 HV. The tool dimensions and geometry are given in Fig. 1. A tool tilt angle of 2° was used during all welds. Over the course of the experiments the tool wear condition can be regarded as constant, due to the tool changes for each new alloy and the comparatively low welded distances per alloy (AW5754 ~ 28.2 m, AW7075 ~ 30.4 m, AW6005 ~ 11.4 m).

The used parameter ranges for welding feedrate and spindle speed (RPM) aimed to evaluate a broad spectrum of industrially applicable parameters within the limits of the machining centers' load capabilities (axial load) and workpiece material properties. The selected parameter combinations facilitate an examination of the primary variables influencing measurable force feedback and the resulting deviations in weld exhibiting defects.

The primary force oscillation at the frequency corresponding to tool rotation primarily results from the superposition of radial tool runout, discontinuous material transport, and geometric tool pin features [34]. Oscillation amplitude

Table 1 New and continued aspects regarding methodology and evaluation within this paper

New aspects to this paper	Methodology and proceedings carried over from previous works
High granularity spindle-integrated process force measurement system	DenseNet-CNN for data classification
Reduction of measurement data-channels, no torque measurements for evaluation	Adjustment of classification threshold by modification of cost function to prevent false negative classifications
Longer welds with up to five changes in plunge depth and three defective areas of differing length per weld	Generation of weld data set across multiple alloys and numerous welding parameter combinations classified by digital micro focus radiographic images
Completely new data set, including new alloy with specific material properties	Meta-data use to scale CNN output for generalization across weld-parameters and alloys
Higher welding speeds (up to 4200 mm/min) than before	
Evaluation of reliability diagrams and binning based on defect prediction value	

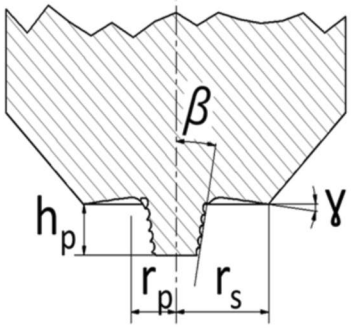

Probe Radius r_P	1.5 mm
Shoulder Radius r_S	4.0 mm
Conical Probe Angle β	10 °
Probe Length h_P	1.42 mm
Concave Shoulder Angle γ	7 °
Pin Feature	Metric thread

Fig. 1 Cross-section drawing and relevant dimensions of used welding tools

is driven by temperature dependent material resistance to extrusion in stir zone and thermomechanical affect zone as well as parameter dependent extrusion volume per tool rotation. The parameter combinations were chosen to examine these influences. 27 different parameter combinations were successfully welded across the three alloys. The combinations are shown in Fig. 2, with marker shape and color indicating the alloy.

Similar to previous efforts, the welding parameter combinations are generally organized in three groups. The first group is characterized by a fixed pitch of 0.5 mm feed per tool revolution, going from 600 to 3600 RPM. The second and third set are based on fixed RPM to evaluate the increase in static forces and oscillation amplitude with increases in welding speed. For AW7075 the spindle speeds are 1200 and 1800 as further increases lead to surface galling and therefore unwanted surface defects. The maximum welding speed was limited by the ability to reliably produce defect free welds. For the other two alloys higher spindle speeds could be utilized and higher welding speeds achieved for defect free welds. To obtain a sound and balanced dataset the lower spindle speed parameters were equal to those of AW7075 and the second set was welded at higher federate and spindle speed. The maximum welding speed was again limited by achieving defect free welds. AW6005 was used to extend the dataset to include a third alloy, overall a lower number of welds was performed to later evaluate generalization capabilities.

FSW welds are typically executed using closed loop axial (Z-axis) force control, to compensate for variations in workpieces and fixtures in industrial production environments. The used machining center does currently not offer that option, therefore welds were produced in position control mode, which in combination with rolled plates of consistent thickness results in superior reliability and reproducibility of plunge depth. This control strategy also mitigates the effects of lag, set force deviation, machine-induced z-axis oscillation, and drift within the recorded data by removing the closed-loop force control system. The reduction in systemic variance enhances the reliability and reproducibility of producing defect-free welds and welds containing inner volumetric defects for each parameter combination. During pretrials, two plunge depths were experimentally determined for each combination of alloy and parameters to achieve both defect free welds and welds without outer defects, but internal void defects. Defects were induced through a reduction in tool plunge depth and resulting decreases of heat input and forging pressure, producing welds with inner

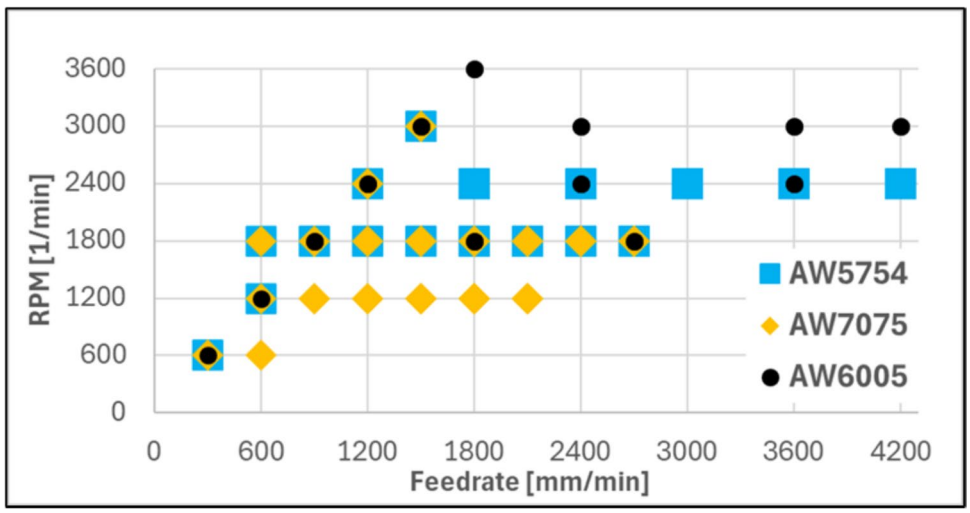

Fig. 2 Welding parameter combinations for each workpiece alloy

volumetric defects while avoiding visually detectable surface and root defects. The plunge depth was varied within each weld through a ramp of two second length, ramp length was reduced to one second for welds faster than 3600 mm/min. Welds 1800 mm/min or faster contained only one ramp changing depth. These welds were performed with both plunge depth change directions. Slower welds contained up to 5 changes in plunge depth within the weld resulting in alternating defective and defect free areas. The plunge depths and an image of the weld surface are shown for two different welding speeds in Fig. 3. Each weld was repeated a different number of times according to the welding speed to obtain 35–41 segments of three seconds length of usable recorded data.

During FSW, the spatial forces were measured using the spindle-integrated real-time force measurement system SpindleForce. The system includes a total of six eddy-current sensors mounted directly in the spindle housing, three arranged axially and three radially, that measure, in a contactless manner, the distance from the sensor head to the target, which in this case is the surface of the HSK63A tool interface. To calculate the relative displacement from the measured sensor signals, the geometrical deviations of the measurement target are compensated by determining the runout of the spindle shaft. The runout is measured in the load-free state, with the spindle angle positions simultaneously acquired using the integrated main spindle encoder. Since the thermal growth of the main spindle components also influences the measurement of the force-induced displacement, this part of the measurement signal is compensated using the method presented in [35]. After compensation of the geometric deviations of the measurement target and the thermal growth of the spindle components, the process-force related relative displacement can be obtained. The calculation method of the relative spindle shaft displacements in axial and radial directions is presented in detail in [36]. Based on the calculated relative displacement of the spindle shaft, the process force can be calculated with the known transfer characteristics between the tool center point and the measurement section. This calculation is based on the input disturbance observer, which is methodically presented in [37]. The input disturbance observer accounts for effects that influence the structural-dynamic characteristics of the spindle, such as tool geometry, rotational speed, force level, and thermo-elastic behavior.

The accuracy of the measurement system strongly depends on the structural stiffness between the tool center point and the measurement section. For the spindle used in this study, the accuracy of the measurement system can be described for the specific working point and different frequency ranges (dynamic 0–2000 Hz and quasi-static 0–50 Hz) for the applied tool by defining the force measurement sensitivity, the accuracy for both is given in Table 2.

The main spindle system with integrated measurement System SpindleForce produced by the Innomotics GmbH is mounted into the milling machining center Heller HF3500.

Table 2 Sensitivity for different frequency ranges of the used process force measurement system

Sensitivity (0–2000 Hz)	Sensitivity (0–50 Hz)
< 20 N (0.083 µm)	< 5 N (0.03 µm)

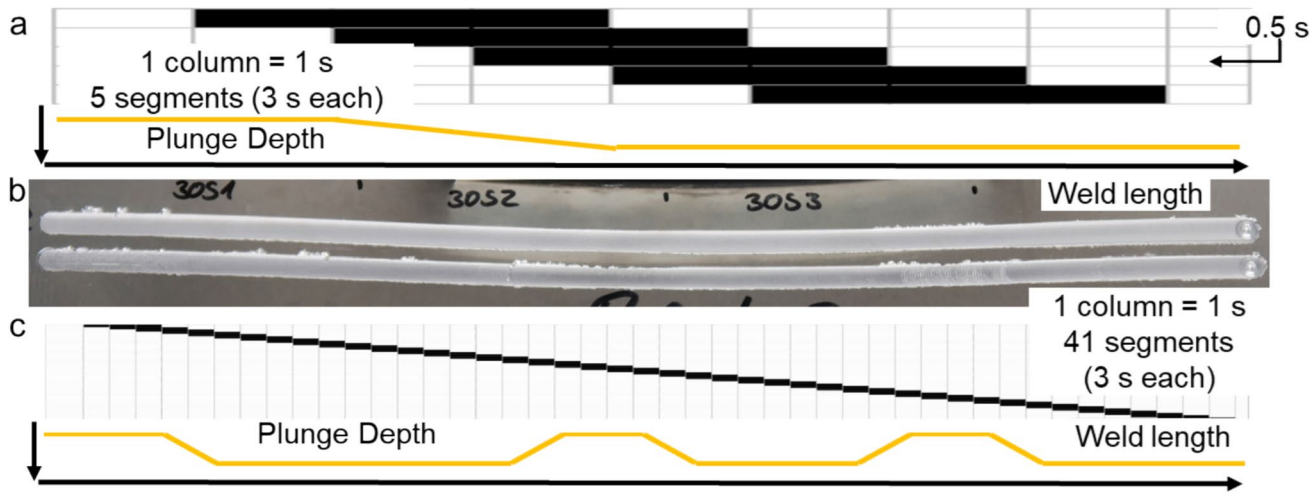

Fig. 3 a) Weld and data-segments at 3000 mm/min; b) Picture of welds in a and c; c) Weld and data-segments at 600 mm/min

3 Results and discussion

3.1 Welding results, classification and dataset

The welds were executed as described above and the data recorded. After FSW some welds were eliminated from evaluation through visual inspection, due to surface galling or surface breaking cavities. The total number of welds was reduced to 134 (AW7075: 51, AW5754: 59, AW6005: 24). To quantify the resulting weld seam quality and localize internal volumetric defects, the specimens were analyzed using radiographic testing (RT). The RT was performed on a digital micro-focus computed tomography machine, Procon CT-ALPHA with a micro (μ)-tube. In micro-focus tomography, X-rays are generated from a single spot source directed toward the detector, with opening ray paths facilitating magnification of the imaged specimen. The rate of magnification is thereby determined by the chosen distance between source, specimen, and detector and directly proportional to the detectable defect size [38, 39]. To obtain high-resolution images with a small defect-detection threshold for the long and narrow welds, specimens were cut into four sections of 115 mm length each, including plunge and tool exit location. The digital images were subsequently compounded to restore the weld image. A duplex wire indicator in accordance with ISO 19232–5, also known as Image Quality Indicator (IQI), was added to the images to accurately determine the detectable size of volumetric defects [40]. The detection threshold established for voids and tunnel defects (internal volumetric defects) was 0.08 mm parallel to the weld surface (D11, ISO 19232–5). This detection threshold exceeds those typically achieved by quality control measures in industrial applications. Along the weld length another wire indicator with consistent mm-based step length was positioned for easy location determination in regards to the weld length. To detect small defects, brightness and contrast adjustments were made on the digital images during post-processing. For the weld classification the adjusted images underwent manual analysis to detect, locate, and mark internal weld defects. The plunge and tool exit locations were excluded from analysis. The annotated images with defect location data were used to label the weld data for NN training. Weld data labeling was performed on a per 3 s weld data segment (Fig. 3) bases, any segment containing a detectable defect of any detectable length (~ 0.08 mm) was classified as containing a defect, class 1 (positive class, defect detected) and data segments containing no detectable defect were label as class 0 (negative class, no defect detected). The RT image analysis was validated through the examination of micro-sections. Multiple cross-sections were cut from various locations of selected welds, including areas free of defects and areas with internal volumetric defects. The resulting classification was in good accordance with the RT image analysis, qualifying the selected method and machine for the weld classification.

For the development of an applicable inline quality monitoring solution with a capability of localizing defects through data analysis, the welds and respective recorded data were divided into shorter segments. Each second of welding time a new segment begins and lasts for three seconds, thereby overlapping the previous and subsequent segment by one second each. This weld segmentation and resulting data structure is shown for two different welding speed in Fig. 3a and 3c. The segment length was determined within prior developments, enabling high classification rates. The overlapping of segments was introduced to increase accuracy by enabling multi-context evaluation of each data point, as the differing data contexts for evaluation allow for feature relation across multiple different folds and broader detection of relevant features, supporting generalization. The overlapping of the segments increases the amount of training data by repeating each data point, compared to consecutive 1 s segments, but the efficient NN implementation still allows for fast training cycles and near real time (~ 2/100th s) inferencing. Compared to consecutive 3 s segments the overlapping of the segments allows for better localization of defects and an increase in detection reliability through multi context evaluation. Regarding the given dataset, the weld length of each segment and thereby the area in which defects start or end, if classified correctly, is reduced from a maximum length of 210 mm to 70 mm (at 4200 mm/min feed rate). The overlapping segmentation expands the amount of available training-data and enables multi-context evaluation for each data-point, improving generalization and defect detection threshold determination.

At the measurement frequency of 2.5 kHz each three second segment of data includes 7500 points of process-force data for each spatial direction, resulting in 22.5k data-points for analysis per weld segment. The data acquisition frequency was derived from previous developments. At 2.5 kHz it allows for the DL development of discernable classification features within the selected segment and especially filter length, while requiring comparatively low computational effort in training and inferencing. At the maximum used spindle speed the acquisition rate still offers > 40 data points pers tool revolution, which enables clear mapping of the process force data of relevant changes of the process compared to an idealized process.

The weld length and maximum feedrate served as references to determine the maximum number of segments for each weld. At the weld length of 440 mm, between 4 (4200 mm/min welding speed) to 41 (600 mm/min) segments could be extracted per weld, while excluding the

last 0.5 s per weld and the first half of welds performed at 300 mm/min to maintain a balanced dataset. Based on RT image labeling, defect identification, and localization, each segment of the welds was classified. Classification was based on the presence of internal void defects within a segment versus segments without detectable defects. For NN training and evaluation, class determination was adapted to a weld segment classification system where the positive class 1 indicates NOK welds (defect detected), while the negative class 0 signifies OK welds (no defect present within the weld seam segment). The final dataset size and classification of 134 welds (AW7075: 51, AW5754: 59, AW6005:24) separated into 1703 segments of weld data is shown in Table 3 on a weld segment base.

3.2 Adaption, training, testing, and validation of neural networks

As the current developments are a continuation of the research, the reasoning behind the selection of densely connected CNN (DenseNet) [41] for this classification task has been extensively discussed in [2, 3]. Furthermore, the adaptations of the original architecture, the addition of meta-data inputs and the modification of the cost function to prevent false negative classification have been presented. A detailed description of the computer hardware used for network training (Nvidia RTX 3090) and network training times related to network widths and learnable parameter counts can be found in chapter 3.2 of [2]. In this study the optimized Network configurations K16T32 and K16T+, which previously showed the highest classification accuracies were used. The exact NN configurations utilized for this research are given in Fig. 4.

The networks were adapted to three input channels for the spatial forces, as no torque was measured. Layer counts, filter sizes and step length were carried over from previous developments. Meta-data channels and input scaling remained consistent with the previous developments. Furthermore, the cost-function developed in [2] for predicted value adjustment to prevent false negative classifications was used. Hyper parameters for the NN training as well as the parameters adjusting the predicted value and threshold were tuned to match the new dataset and defect classification. The configuration of the NN as well as the average resulting classification accuracy and positive factor of summed up misclassifications of the test set data (10% of data-set, 170 observations) of n = 3 training iterations (total of 510 data-segments) are shown in Table 4. The positive factor (P_f) has been previously established (compare [2]) to measure the success of the threshold modification and relate the shift to overall accuracy. It relates the number of false negative classifications to the number of false positive classifications and offers significant insight for performance comparison when presented alongside overall accuracy. It is established this way, as division by the targeted number of 0 false negatives is not possible and will be denoted as the given fraction and not the calculated value in cases of 0 false negative classifications. The formula is given in Eq. 1.

$$\textit{Positive factor}: \; P_f = \frac{\text{number of false negative}}{\text{number of false positive}} = \frac{t - y = 1}{t - y = -1} \tag{1}$$

Eq. (1).

The achieved accuracies are overall lower than in previous publications. The reduction is based on the absence of torque data, which has been shown to relate well to material transport and reduces the learnable dependencies between lateral force oscillation, axial force and torque. As before, the accuracies show the better result for the network configuration with less learnable parameters. Over three trainings iterations 10 of 510 segments were misclassified, with one being a false negative. The wider network was slightly less accurate, misclassifying 14 of 510 segments, however, as shown in previous publications, the generalization and threshold determination benefit from an increase in classification features, resulting in 0 false negative classifications on a dataset with 80 weld segments containing defects, and 90 defect free segments. The summed-up confusion matrices of n = 3 network trainings are shown in Fig. 5.

The detailed confusion matrices that analyze the data from Fig. 5 on a per alloy basis are given in Fig. 6. The indicated differences in accuracy across the different alloys are low and in good accordance with overall accuracy showing a good fit of the trained model for the classification task.

Further analysis of the one critical false negative misclassification (AW5754, K16T32) shows that the not detected

Table 3 Number of weld segments per alloy and classification label

Dataset	Full set	AW7075	AW5754	AW6005
Class 0: defect free segment	787 46.21 %	346 46.51 %	301 46.81 %	140 44.30 %
Class 1: volumetric defect segment	916 53.79 %	398 53.49 %	342 53.19 %	176 55.70 %
Sum	1703	703	643	316

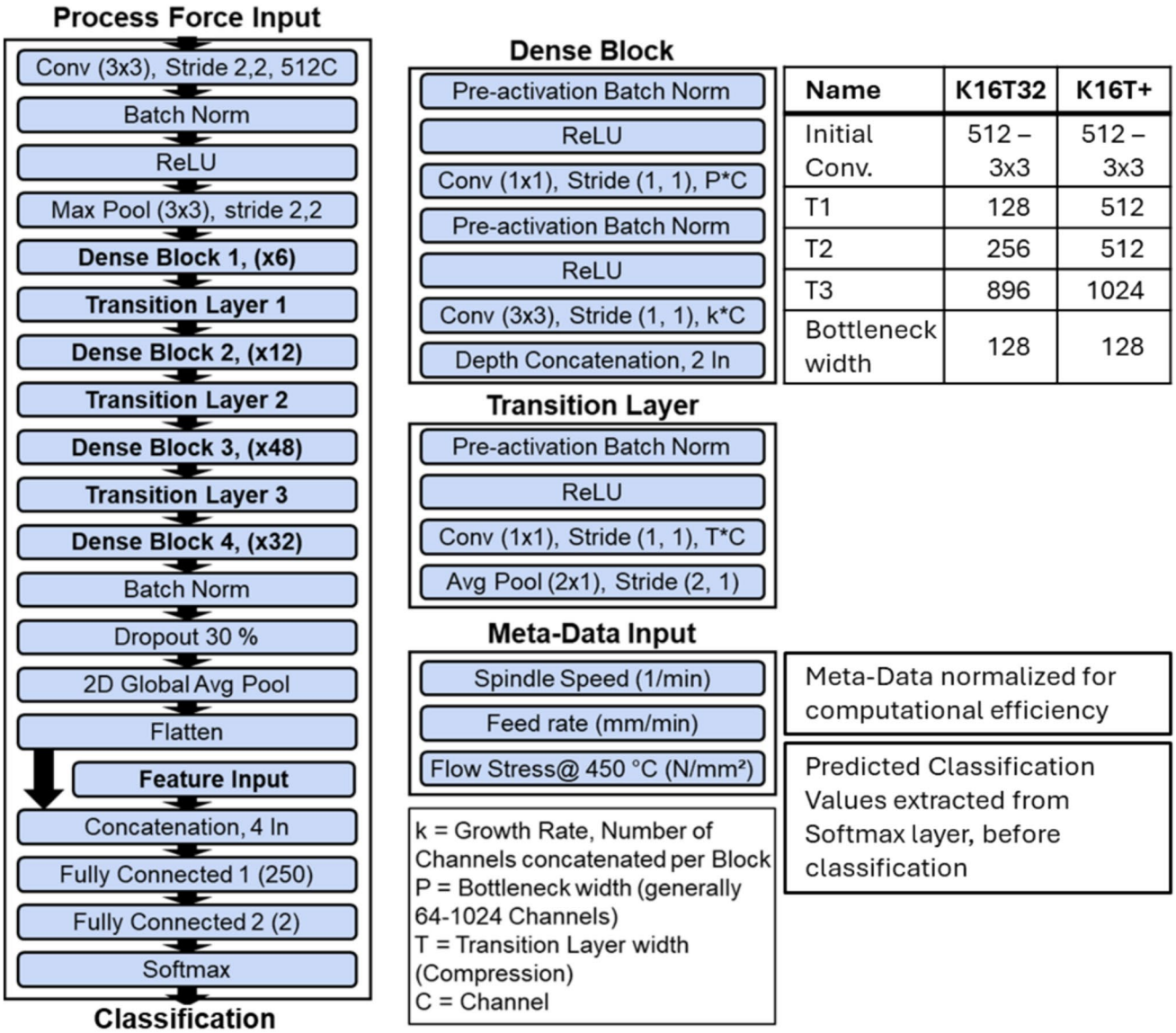

Fig. 4 DensNet-CNN configuration and modifications for FSW weld-data classification

Table 4 Network configuration and resulting average classification accuracy (n = 3)

Network configuration	K16T32	K16T +
Initial convolution	512*3 × 3	512*3 × 3
Transition-layer T1, T2, T3	128, 256, 896	512, 512, 1024
Bottleneck width (P)	128	128
Positive factor (P_f), n = 3	**0.111**	**0/14**
Classification accuracy [%], n = 3	**98.04**	**97.25**
Acc. [%] iteration 1	98.24	96.47
Acc. [%] iteration 2	98.24	98.24
Acc. [%] iteration 3	97.65	97.05

defect is the beginning of an internal void defect. While the data-segment is labeled as defective, because it contains a defective area, the defect area within the data-segment is only about 0.25 s of the 3 s data segment. Both consecutive segments, which contain these misclassified 0.25 s are classified correctly, identifying the defect through the following data or features generated by the relations of data, which provides a clear indication of the defect. The data of the relevant weld is shown in Fig. 7. The segmented data is given in Fig. 7 b-d, with segment b showing the false negative classification based on 0.25 s of data corresponding to an identified defect. At the given welding speed of 2700 mm/min the 0.25 s time is equal to 11 mm of weld distance. The true positive classifications of data segments in Fig. 7 c and

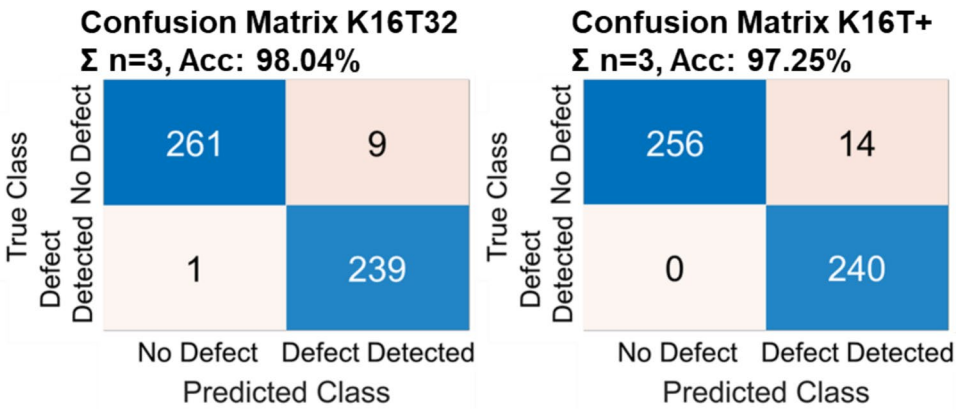

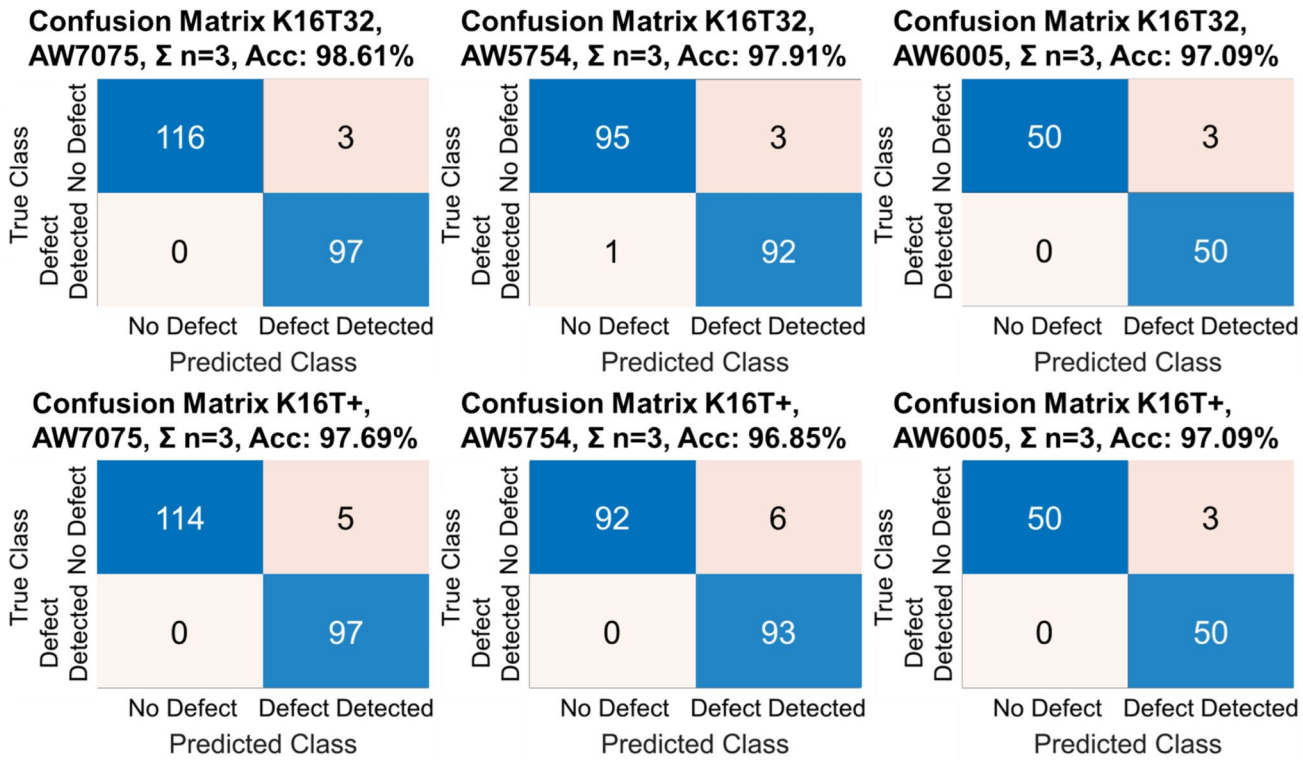

Fig. 5 Summed up confusion matrices (n = 3) for both network configurations

Fig. 6 Confusion matrices (n = 3) of each alloy for both network configurations

d enable the correct identification of the defect with a location error of 11 mm distance from the expected 45 mm weld length (1 s at 2700 mm/min) segment of the position of the segment first detecting the defect.

When analyzing the false positive classifications spiking oscillations of lateral forces can be identified in nearly half. The spiking oscillation is characterized by an additional oscillation of the upper threshold of the oscillation amplitude while the lower threshold remains nearly constant. True positive classifications are often characterized by increased or erratic oscillation amplitudes of the lateral force. Generally, this includes variations in the upper and lower threshold of the amplitude. For the remainder of misclassifications no indication for the underlying reasons could be identified when manually analyzing the data and resulting force graphs.

14 of the 23 false positive and the one false negative misclassification occur in data segments containing a change in plunge depth and are therefore physically close to the beginning or the end of a nearby internal void defect. This indicates challenges in determining a generalized defect detection threshold over the wide range of used welding parameters and alloys. The derived detection threshold over classifies defects for some weld parameter combinations.

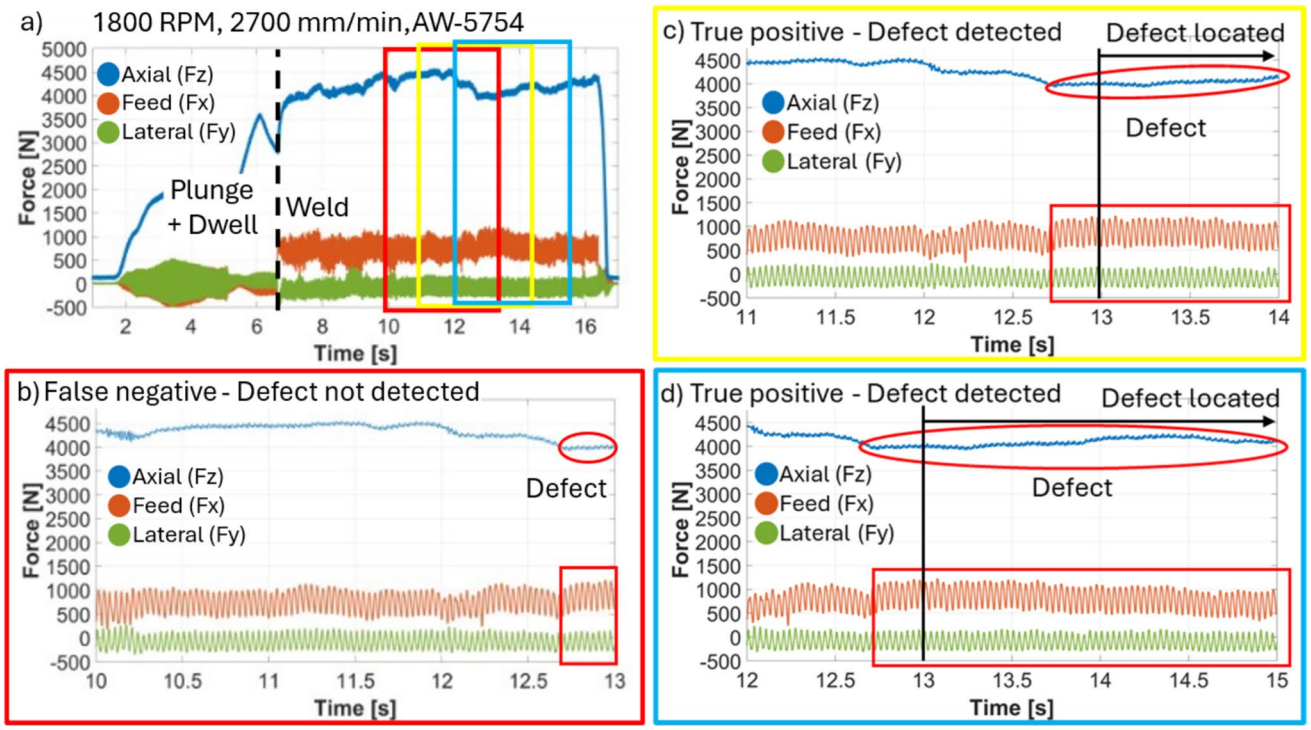

Fig. 7 Segmented welding data of false negative classification, two consecutive data segments and defect localization

The same results can be derived from the reliability diagrams of the investigated CNN configurations, which are shown in Fig. 8. The network predictions were separated into 10 bins based on the predicted value and the mean values of the bin predictions plotted against the relative frequency of true positive class occurrences within the bin. Along with the prediction data, the number of observations in each bin was plotted.

Based on Fig. 8 it can be deduced that the model falls considerably short of the conventional definition of a "perfectly calibrated" model, particularly for the bins within the 0.1–0.9 mean prediction values. Along with the low number of observations within these bins, the significant influence exerted by the adjustment of the cost function is illustrated. The relative frequency of positive class classifications is further skewed due to the limited total number of instances available, which diverges substantially from the anticipated ideal calibration. Instances where the target values are 0 yet result in predictions > 0 signify an additional impact of the cost function modification, which serves to elevate the average classification value closer to that of the positive class. This is validated when comparing predicted value and mean relative frequency of the positive class. The mean predicted value generally exceeds the mean relative frequency due to the cost function modification, which penalizes false negative classifications significantly stronger than false positives.

These findings demonstrate the complexity involved in achieving adequate model calibration and highlight the impact of cost function modification on overall classification performance for the application of quality monitoring. Overall the results demonstrate that the model is well fit for the quality monitoring task, by pushing predicted values close to absolute 0 or 1 predictions (88.43% of prediction < 0.1 or > 0.9) and balancing classification accuracy with the prioritization of defect detection over false negatives.

To validate the achieved results a "leave one domain out" investigation was performed. The data set was separated and all data segments of welds in AW5754 and AW7075 were used for the NN training, while the data segments of the AW6005 were used as the test data. AW6005 was chosen as it is the smallest partial data set containing 316 of the 1703 observations. The resulting classification accuracy and defect detection rate for the alloy left out of training are in good accordance with the results achieved within similar validation experiments during previous research [2]. An overall classification accuracy of 87.97% was achieved. The confusion matrix is shown in Fig. 9, along with the reliability plot and an event level analysis. It is assumed that the significant increase in misclassifications is based on the faulty scaling of detected features relevant to classification, especially due to the comparably low flow stress meta-data of AW6005, which is outside (lower at 450 °C) the flow stress range included in the training data set. The

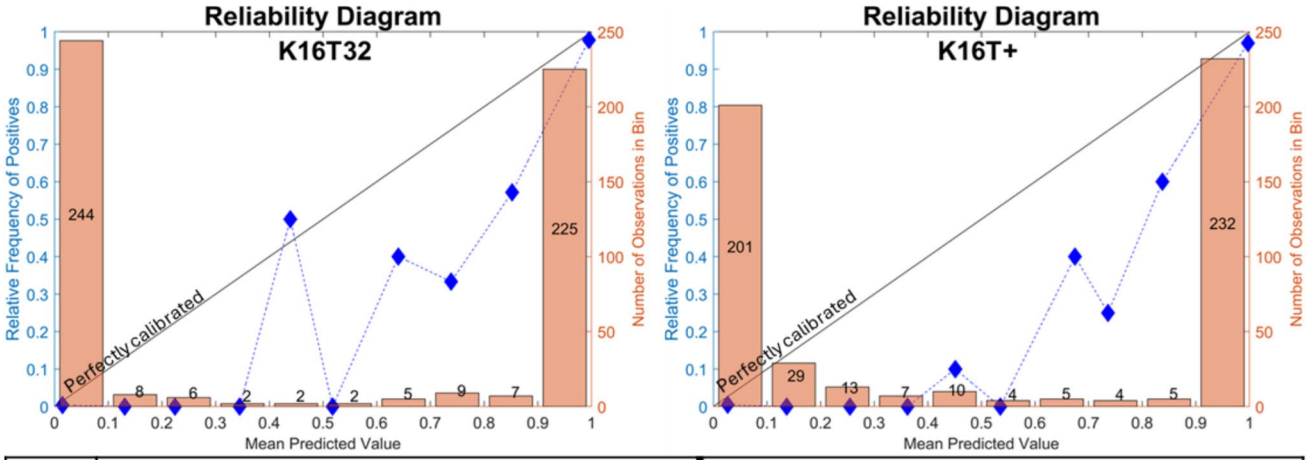

	Data of K16T32 Reliability Diagramm			Data of K16T+ Reliability Diagramm		
	Mean Prediction	Rel. freq. of pos class in labels	Total number of pos. class in bin	Mean Prediction	Rel. freq. of pos class in labels	Total number of pos. class in bin
Bin1	0.0148	0.0041	1	0.0267	0.0000	0
Bin2	0.1307	0.0000	0	0.1366	0.0000	0
Bin3	0.2242	0.0000	0	0.2547	0.0000	0
Bin4	0.3448	0.0000	0	0.3622	0.0000	0
Bin5	0.4391	0.5000	1	0.4512	0.1000	1
Bin6	0.5179	0.0000	0	0.5352	0.0000	0
Bin7	0.6403	0.4000	2	0.6746	0.4000	2
Bin8	0.7386	0.3333	3	0.7363	0.2500	1
Bin9	0.8519	0.5714	4	0.8376	0.6000	3
Bin10	0.9951	0.9778	220	0.9971	0.9698	225

Fig. 8 Reliability diagrams (mean values/total observations in bins for n = 3) and complementary data for 10 bin classification reliability investigation both network configurations

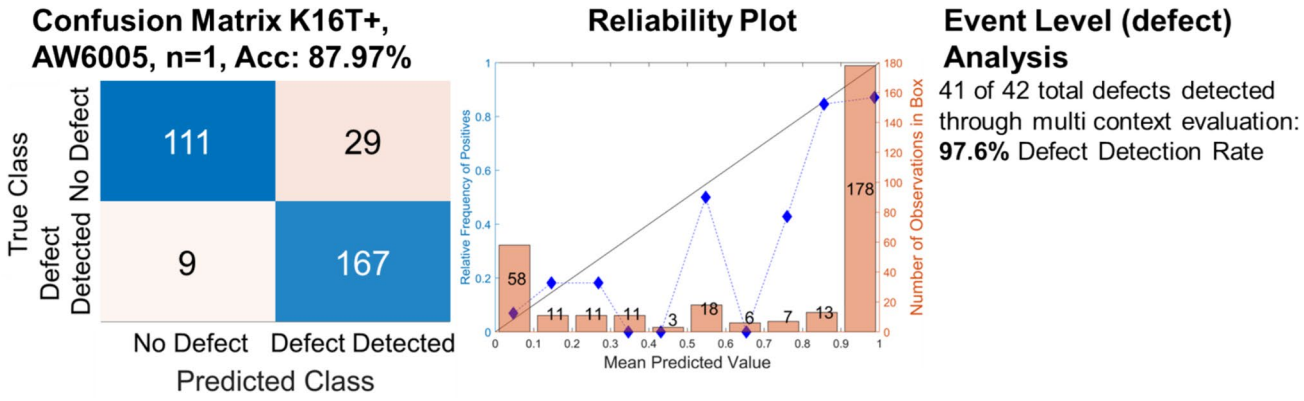

Fig. 9 Confusion matrix, reliability plot and event level defect analysis

reliability plot of the predicted values for the positive class shows higher uncertainty of the predictions than Fig. 8, with a significant number of defect free welds spread out across higher bins with mean predictions up to 0.6. Despite the increased uncertainty of the predictions the defect detection threshold shift is still evident within confusion matrix and

reliability plot, resulting in a positive factor of 0.31. When analyzing the test data set on an event-based level (defect detection), 41 of 42 defects within the welds are correctly detected, resulting in a 97.6% defect detection rate. The percentage being vastly dependent on the low number of occurrences. The undetected defect is located at the end of a weld and only 2 data segments contain parts of the defect, both including the plunge depth ramp. The other seven false negatives are all located within plunge depth ramps and only contain small parts of defects within the 3 s data segment, similar to Fig. 7b.

4 Application for inline quality control

The network classification accuracies obtained from the training of the modified DenseNets with the recorded dataset demonstrate an advantage over conventional defect detection methods used in industry. The developed system can be used as near real-time inline quality control. Furthermore, it eclipses methods such as ultrasonic testing, radiographic testing, and visual inspection in terms of the size of detectable defects, cost efficiency and production time [11, 42–45]. Initial validation results indicate a potential limitation in the developed system's applicability due to classification accuracies between 88 and 98% for generalized tasks. For the inline quality monitoring, however, the defect detection rate substantially surpasses the classification accuracy. The improvement results from multi-context evaluation of the staggered data-segments. Most misclassifications occur within the defect transition zones, with only isolated weld segments being incorrectly classified. For the developed dataset across all NN training iteration (n = 6) all internal void defects were successfully detected due to the multi context evaluation, with only the start point of one not being localized properly. The single false negative classification of the testing data has been discussed on the previous chapter. Based on the presented confusion charts and the correct defect detection by overlapping segments of data, 100% of defects were correctly identified in the testing data. The same holds true for the training data. While the total number is of false negatives is higher (10) the overlapping evaluation also generates a 100% defect detection rate during the six evaluated training cycles and 10,218 used data-segments. During "leave one domain out" validation, accuracies of 87.97% with defect detection rate of 97.6% were achieved, when classifying an alloy with mechanical properties outside the training data range. The accuracy and defect detection rate are comparable to alternative quality control methods. However, since higher rates can be achieved, it cannot be recommended to utilize the system without expanding the training data set to include labeled welds with the chosen material properties.

The developed system, based on a robust, high granularity process data recording system is capable of real time process data recording. The recorded process data is supplemented with meta-data related to the welding parameters and workpieces. The developed evaluation algorithm can be implemented on an edge device and deliver quality indication in near real-time, giving localized ROI at up to less than 2% error rate for further defect investigation. While achieving high classification accuracies and 100% defect detection, the classification results are up to 2.5% worse, when compared to previous implementations which utilized a different measurement system that included torque measurements. In FSW tool torque is directly related to energy input and material intermixing and can therefore provide important information regarding the process, especially in conjunction with the process forces and information regarding the welded components. Based on these facts and the results achieved with the presented dataset the inclusion of direct torque measurement for any industrial implementation is strongly recommended to increase accuracy and improve stability.

Data inferencing of segmented process-data (3 s segment length) can be performed at low computational cost in ~ 2/100 s (on a laptop computer with 6th gen Intel i5 and 8 GB of RAM) and even faster on dedicated edge TPUs (tensor processing units). An evaluation of the recorded data is thereby possible in near real time.

This, in conjunction with the quality information, can meet customer requirements for product traceability. In subsequent steps, the system can be enhanced within a fully connected production workshop. This enhancement will enable not only the delivery of localized quality data to downstream processes but also the utilization of data from upstream processes to adjust metadata according to local workpiece properties and current tool and machine quality information.

At the current stage of development the state of tool wear is not included in the quality evaluation. Tools utilized for data-set generation are in generally good condition and only used for sub 50 m of weld distance. It is known that geometric wear influences the occurrence of process forces, especially the base value and amplitude of the in-plane welding forces (feed force and lateral force). Therefore, further experiments will need to be conducted to include the tool wear state in the quality evaluation. It is to be determined whether the state of wear can be integrated into the general evaluation data, or if adding the wear state as a feature data input through either welded distance or fraction of tool life expectancy is the most effective solution.

5 Conclusion

Within this work convolutional neural networks based on DenseNet201 were modified and weld-parameter and workpiece meta-data was concatenated to scale features detecting internal void defects based on transient process data and enhance generalization. The networks were trained to detect internal void defects based on welding data recorded by a robust, high granularity spindle integrated force measurement system. For a dataset of 1703 weld seam segments from three different alloys and 27 different feedrate and spindle speed combinations average classification accuracies of > 98% were achieved. The modification of the cost function proved effective again, shifting the positive factor over six trainings iterations to 0.04. However, the number of false positive ROI indications shows the challenges in determining a generalized defect detection threshold, even when utilizing meta-data for feature scaling. The achieved accuracy is lower than in previous works, due to the lack of torque measurement data, which allows for the identification of material transport through evaluation of interdependencies between the spatial forces and tool torque.

The performed validation experiments, removing on alloy from the data set and using it as test-data, showed a significant drop in classification accuracy to 87.97%, which is assumed to be mostly based on the meta-data base feature scaling of the material flow stress which is outside the training data flow stress range. The trained network still achieved a defect detection rate of 97.6% (41 of 42) for the new alloy, which is comparable to most NDE techniques. These results suggest that while the system is capable of quality monitoring and defect detection even for welds in alloys outside its training property range, including data containing all mechanical properties will yield better and more reliable results.

Despite the lower classification accuracy, the staggered data-structure and multi-context evaluation allow for a detection rate of 100% of the targeted internal volumetric defects when evaluation data is within the training data set range. The used data-recording system provides weld-force data in real-time allowing for near real-time evaluation (~ 0.2 s delay) and integration of the light-weight evaluation algorithm at the edge. Furthermore, the recorded data, amended with meta-data and quality information can be used in connected production environments, integrating upstream production data providing downstream quality information, while allowing for complete production traceability.

Authors contributions All authors contributed to the study conception and design. Material preparation, data collection and analysis were performed by P. Rabe and A. Strachkov. The first draft of the manuscript was written by P. Rabe and A. Strachkov and all authors commented on the manuscript. All authors read and approved the final manuscript.

Funding Open Access funding enabled and organized by Projekt DEAL. Funded by the Deutsche Forschungsgemeinschaft (DFG, German Research Foundation) under Germany's Excellence Strategy – EXC 2023 Internet of Production – 390621612.

Data availability Recorded Data available from the authors upon reasonable request.

Declarations

Competing interests The authors declare that there exists no competing financial interest or personal relationships that could have appeared to influence the work reported in this paper.

References

1. Brecher C, Schuh G, van der Aalst W, Jarke M, Piller FT, Padberg M (2024) Internet of Production. Cham: Springer International Publishing.https://doi.org/10.1007/978-3-031-44497-5.ISBN: 978-3-031-44496-8
2. Rabe P, Schiebahn A, Reisgen U (2025) Development and validation of a generalized, AI-based inline void defect detection solution for FSW based on force feedback. Weld World 69(2):499–514. https://doi.org/10.1007/s40194-024-01895-2
3. Rabe P, Schiebahn A, Reisgen U. Volumetric defect detection in friction stir welding through convolutional neural networks generalized across multiple aluminum-alloys and sheet thicknesses. In: Proceedings in Engineering Mechanics. 43–61. https://doi.org/10.1007/978-3-031-54732-4_4
4. Rabe P, Reisgen U, Schiebahn A (2023) Non-destructive evaluation of the friction stir welding process, generalizing a deep neural defect detection network to identify internal weld defects across different aluminum alloys. Weld World 67(3):549–560. https://doi.org/10.1007/s40194-022-01441-y
5. Rabe P, Schiebahn A, Reisgen U (2022) Deep learning approaches for force feedback based void defect detection in friction stir welding. J Adv Join Process 5:100087. https://doi.org/10.1016/j.jajp.2021.100087
6. Rabe P, Schiebahn A, Reisgen U (2021) Force feedback-based quality monitoring of the friction stir welding process utilizing an analytic algorithm. Weld World 65(5):845–854. https://doi.org/10.1007/s40194-020-01044-5
7. Thomas WM et al. Improvements relating to friction welding. European Patent Specification 0615 48 B1
8. Lohwasser D, Chen Z (2010) Friction stir welding: from basics to applications. WP Woodhead Publishing, Boca Raton, FL
9. Richter B (2017) Robot-based friction stir welding for E-mobility and general applications. eBIS 2017(5):103–110. https://doi.org/10.17729/ebis.2017.5/11

10. Sharma N, Khan ZA, Siddiquee AN (2017) Friction stir welding of aluminum to copper—an overview. Trans Nonferrous Met Soc China 27:2113–2136. https://doi.org/10.1016/S1003-6326(17)60238-3
11. Taheri H, Kilpatrick M, Norvalls M, Harper WJ, Koester LW, Bigelow T et al (2019) Investigation of nondestructive testing methods for friction stir welding. Metals 9(6):624. https://doi.org/10.3390/met9060624
12. Luhn T (2013) Prozessdiagnose und prozessüberwachung beim rührreibschweißen [Zugl.: Ilmenau, Techn. Univ., Diss., 2012]. Berlin, Pro Business. ISBN: 9783863869632
13. Boldsaikhan E, Logar AM, Corwin EM (2010) Real-time quality monitoring in friction stir welding: The use of feedback forces for nondestructive evaluation of friction stir welding. Lambert Academic Publishing, Saarbrücken (**9783838352985**)
14. Mishra D, Roy RB, Dutta S, Pal SK, Chakravarty D (2018) A review on sensor based monitoring and control of friction stir welding process and a roadmap to Industry 4.0. J Manuf Process 36:373–397. https://doi.org/10.1016/j.jmapro.2018.10.016
15. Das B, Pal S, Bag S (2016) A combined wavelet packet and Hilbert-Huang transform for defect detection and modelling of weld strength in friction stir welding process. J Manuf Process 22:260–268. https://doi.org/10.1016/j.jmapro.2016.04.002
16. Brecher C, Eckel H-M, Motschke T, Fey M, Epple A (2019) Estimation of the virtual workpiece quality by the use of a spindle-integrated process force measurement. CIRP Ann 68(1):381–384. https://doi.org/10.1016/j.cirp.2019.04.020
17. Mishra RS, De PS, Kumar N (2014) Friction stir welding and processing: Science and engineering. Springer, Cham, Heidelberg. https://doi.org/10.1007/978-3-319-07043-8 (**9783319070421**)
18. Gebhard P (2011) Dynamisches Verhalten von Werkzeugmaschinen bei Anwendung für das Rührreibschweißen [Zugl.: München, Techn. Univ., Diss., 2010]. München, Utz
19. Hattingh DG, Blignault C, van Niekerk TI, James MN (2008) Characterization of the influences of FSW tool geometry on welding forces and weld tensile strength using an instrumented tool. J Mater Process Technol 203(1–3):46–57. https://doi.org/10.1016/j.jmatprotec.2007.10.028
20. Hasieber M, Wenz F, Grätzel M, Lenard JA, Matthes S, Bergmann JP (2023) A systematic analysis of maximum tolerable tool wear in friction stir welding. Weld World 67(2):325–339. https://doi.org/10.1007/s40194-022-01407-0
21. Cole EG, Fehrenbacher A, Shultz EF, Smith CB, Ferrier NJ, Zinn MR et al (2012) Stability of the friction stir welding process in presence of workpiece mating variations. Int J Adv Manuf Technol 63(5–8):583–593. https://doi.org/10.1007/s00170-012-3946-1
22. Więckowski W, Burek R, Lacki P, Łogin W (2018) Analysis of wear of tools made of 1.2344 steel and MP159 alloy in the process of friction stir welding (FSW) of 7075 T6 aluminium alloy sheet metal. EiN 21(1):54–9. https://doi.org/10.17531/ein.2019.1.7
23. Muhayat N, Zubaydi A, Sulistijono, Yuliadi MZ (2014) Effect of tool tilt angle and tool plunge depth on mechanical properties of friction stir welded AA 5083 joints. Adv Appl Mech Mater 493:709–14. https://doi.org/10.4028/www.scientific.net/AMM.493.709
24. Zettler R, Lomolino S, dos Santos JF, Donath T, Beckmann F, Lippman T et al (2005) Effect of tool geometry and process parameters on material flow in FSW of an AA 2024–T351 alloy. Weld World 49(3–4):41–46. https://doi.org/10.1007/BF03266474
25. Fehrenbacher A, Duffie NA, Ferrier NJ, Pfefferkorn FE, Zinn MR (2014) Effects of tool–workpiece interface temperature on weld quality and quality improvements through temperature control in friction stir welding. Int J Adv Manuf Technol 71(1–4):165–179. https://doi.org/10.1007/s00170-013-5364-4
26. Franke D, Rudraraju S, Zinn M, Pfefferkorn FE (2020) Understanding process force transients with application towards defect detection during friction stir welding of aluminum alloys. J Manuf Process 54:251–261. https://doi.org/10.1016/j.jmapro.2020.03.003
27. Roberts J (2016) Weld quality classification from sensory signatures in Friction-Stir-Welding (FSW) Using discrete wavelet transform and advanced metaheuristic techniques. LSU Master's Theses
28. Hattingh DG, van Niekerk TI, Blignault C, Kruger G, James MN (2004) Analysis of the FSW force footprint and its relationship with process parameters to optimise weld performance and tool design. Welding World 48(1–2):50–58. https://doi.org/10.1007/BF03266414
29. Boldsaikhan E, Corwin EM, Logar AM, Arbegast WJ (2011) The use of neural network and discrete Fourier transform for real-time evaluation of friction stir welding. Appl Soft Comput 11(8):4839–4846. https://doi.org/10.1016/j.asoc.2011.06.017
30. Jene T (2008) Entwicklung eines Verfahrens zur prozessintegrierten Prüfung von Rührreibschweißverbindungen des Leichtbaus sowie Charakterisierung des Ermüdungsverhaltens der Fügungen [Zugl.: Kaiserslautern, Techn. Univ., Diss., 2008]. Techn. Univ. Lehrstuhl für Werkstoffkunde
31. Boldsaikhan E, Corwin EM, Logar A, Arbegast WJ (2006) Neural network evaluation of weld quality using FSW feedback data. In Proceedings of the 6th International Friction Stir Welding Symposium, Saint Sauveur, QC, Canada, 10–13 October 2006
32. Hartl R, Bachmann A, Habedank JB, Semm T, Zaeh MF (2021) Process monitoring in friction stir welding using convolutional neural networks. Metals 11(4):535. https://doi.org/10.3390/met11040535
33. Krizhevsky A, Sutskever I, Hinton GE (2017) Imagenet classification with deep convolutional neural networks. Commun ACM 60(6):84–90. https://doi.org/10.1145/3065386
34. Ambrosio D, Wagner V, Dessein G, Paris J-Y, Jlaiel K, Cahuc O (2021) Plastic behavior-dependent weldability of heat-treatable aluminum alloys in friction stir welding. Int J Adv Manuf Technol 117(1–2):635–652. https://doi.org/10.1007/s00170-021-07754-4
35. Brecher C, Eckel H-M, Fey M. Verfahren zur Erfassung einer axialen Verlängerung einer rotierenden Welle relativ zu einem Gehäuse. European Patent Specification DE102019008025A1
36. Eckel H-M (2024) Kinematische Analyse von Spindellagern unter statischen und dynamischen Kräften [Dissertation]. Aachen, Apprimus Verlag
37. Brecher C, Fey M, Strachkov A (2025) Strukturdynamisches Verhalten der Hauptspindel im Betrieb/Structural-dynamic behavior of the main spindle during machining – Determining the main spindle's structural-dynamic properties based on operating conditions. 115(07–08):593–9. https://doi.org/10.37544/1436-4980-2025-07-08-63
38. Kerckhofs G, Schrooten J, van Cleynenbreugel T, Lomov SV, Wevers M (2008) Validation of x-ray microfocus computed tomography as an imaging tool for porous structures. Rev Sci Instrum 79(1):13711. https://doi.org/10.1063/1.2838584
39. Viscom. X-ray tubes; 2021 [cited 2025 Aug 22]. https://www.viscom.com/en/products/x-ray-tubes/
40. International Organization for Standardization. ISO 19232-5. Non-destructive testing — Image quality of radiographs: Determination of the image unsharpness and basic spatial resolution

value using duplex wire-type image quality indicators. 2018th ed
41. Huang G, Liu Z, van der Maaten L, Weinberger KQ (2017) Densely Connected Convolutional. Networks 1063–6919:2261–2269. https://doi.org/10.1109/CVPR.2017.243
42. See JE. Visual Inspection Reliability for Precision Manufactured Parts. Hum Factors 2015; 57(8):1427–42. https://doi.org/10.1177/0018720815602380
43. Spencer F, United States. Dept. of Transportation, Sandia National Laboratories. Visual Inspection Research Project Report on Benchmark Inspections; 1996 DOT/FAA/AR-96/65. https://doi.org/10.21949/1403546
44. Burford DA, Gimenez Britos P., Boldsaikhan E, Brown J. Evaluation of Friction Stir Weld Process and Properties for Aerospace Application: e-NDE for Friction Stir Processes. National Institute for Aviation Research. Wichita State University, Wichita, KS. FAA Joint Advanced Materials & Structures (JAMS). 6th Annual Technical Review Meeting. 2010
45. Huggett D. Friction Stir Welding Manufacturing Advancement by On-Line High Temperature Phased Array Ultrasonic Testing and Correlation of Process Parameters to Joint Quality [Luisiana State University, Doctoral Dissertation]; 2017. https://doi.org/10.31390/gradschool_dissertations.4139